

# ***F* center in LiF: A quantum mechanical *ab initio* investigation of the hyperfine interaction between the unpaired electron at the vacancy and its first seven neighbors**

G. Mallia,<sup>1</sup> R. Orlando,<sup>2</sup> C. Roetti,<sup>1</sup> P. Ugliengo,<sup>1</sup> and R. Dovesi<sup>1,3,\*</sup>

<sup>1</sup>*Dipartimento di Chimica IFM, Università di Torino, via Giuria 5, I-10125 Torino, Italy*

<sup>2</sup>*Dipartimento di Scienze e Tecnologie Avanzate, Università del Piemonte Orientale "Amedeo Avogadro,"  
Corso Borsalino 54, I-15100 Alessandria, Italy*

<sup>3</sup>*Unità INFN di Torino, sezione F via Giuria 5, I-10125 Torino, Italy*

(Received 21 December 2000; published 10 May 2001)

The paramagnetic *F* center in LiF is investigated at a quantum mechanical level with the CRYSTAL98 periodic code by using a supercell scheme. The isotropic and anisotropic components of the hyperfine coupling tensor describing the interaction between the unpaired electron and the nuclear spins up to the seventh nearest neighbors of the defect are computed by using two different Hamiltonians (Hartree-Fock and local density approximation), and turn out to compare reasonably well with electron paramagnetic resonance and electron-nuclear double resonance data. A term of the hyperfine tensor, not yet available experimentally, is presented for future comparison. The defect wave function is analyzed in terms of the charge and spin density maps, band structure, and Mulliken population.

DOI: 10.1103/PhysRevB.63.235102

PACS number(s): 71.55.-i, 71.23.An, 75.25.+z, 71.15.Nc

## I. INTRODUCTION

*F* centers in alkali halides have been the object of extensive and systematic investigation for more than 60 years; they are produced either by introducing a stoichiometric excess of alkali metal atoms or by exposing the crystal to ionizing radiation, like neutrons,<sup>1</sup> electron bombardment,<sup>2</sup> or x-ray irradiation.<sup>2-7</sup> An *F* center is an electron trapped at a negative-ion vacancy within the crystal; the defective system is paramagnetic, and has been characterized by electron spin resonance techniques, such as EPR (electron paramagnetic resonance) and ENDOR (electron-nuclear double resonance),<sup>4-6,8</sup> since the early 1950s. In this paper we present the first (to our knowledge) periodic *ab initio* quantum mechanical simulation of the *F* center in LiF, including the structural, electronic, and magnetic properties around the defect, with particular attention to the hyperfine coupling tensor *T* between the unpaired electron and the nuclear spin of the Li and F neighbors. Two different Hamiltonians [Hartree-Fock and local density approximation (LDA)] are used, as available in the CRYSTAL98 program,<sup>9,10</sup> in conjunction with a basis set of localized functions and the supercell scheme.

The calculation of properties such as the Fermi contact and the anisotropic component of the hyperfine coupling tensor at an *ab initio* periodic level has become possible only recently. The results obtained for the  $V_{OH}$  center<sup>11,12</sup> in MgO, CaO, and SrO have undoubtedly demonstrated that Hartree-Fock spin density can be so accurate as to reproduce experimental data with excellent agreement. In other more complicated cases, like the compensated trapped hole centers<sup>13,14</sup> in the same alkaline earth oxides, even if not so good, the agreement is semiquantitative. The *F* center defect in LiF, which is examined in the present paper, is particularly interesting as it offers the possibility of extending the analysis of electron-nuclear spin coupling to a fairly large set of neighboring nuclei; in fact, in this case coupling constants

have been obtained experimentally up to the seventh nearest neighbors. This allows a deeper and more severe test of the performance of the methods as regards the Hamiltonian used, the basis sets, and the supercell size.

The paper is organized as follows. Section II is devoted to computational details: basis set, supercell size, accuracy of the calculation. Section III gives the results and their discussion: the electronic structure around the defect is described in terms of Mulliken analysis, charge and spin density maps, band structure, and defect formation energy. Section IV is devoted to the hyperfine coupling tensor at the various neighbors.

## II. COMPUTATIONAL DETAILS

The calculations have been performed with the periodic CRYSTAL98 code.<sup>10</sup> As the system has an odd number of electrons, the unrestricted Hartree-Fock<sup>15</sup> (UHF) and the local spin density approximation<sup>16</sup> computational schemes have been used. As regards the latter Hamiltonian, the adopted exchange and correlation potentials are Dirac-Slater and Perdew Zunger, respectively, indicated as LDA-PZ in the following.

As regards the basis set, Bloch functions are built from localized functions, namely, Gaussian type functions (GTF's) resulting from the product of a Gaussian and a real solid spherical harmonic,<sup>9</sup> or, more generally, from a linear combination (*contraction*) of GTF's. In the following they will be indicated as *atomic orbitals*, AO's. For Li and F, 5 and 13 AO's have been used (resulting from the contraction of six and one GTF's for the *1s* and *2sp* shells of Li, and the contraction of seven, three, one, and one GTF's for the *1s*, *2sp*, *3sp*, and *4sp* shells of F).<sup>17</sup> In order to have an accurate description of the unpaired electron at the vacancy, a basis set has been added corresponding to the "ghost" atom. This basis set will be discussed in the following section, together with the defect wave function. The isolated fluorine atom energy adopted for the evaluation of the defect formation energy is equal to  $-99.37504$  (Hartree-Fock) and  $-99.06440$  (LDA-PZ) hartree and is obtained by using the

TABLE I. Effect of the supercell size on  $E_f^n$ , the defect formation energy (in hartree).  $E_p^n$  is the perfect supercell energy,  $E_p^2$  is the corresponding energy per LiF unit, and  $E_d^{n-1}$  is the defective system energy.  $n$  is the number of atoms in the supercell.  $P$ ,  $F$ , and  $I$  stand for primitive, face-centered, and body-centered lattice.  $E_f$  refers to the unrelaxed defect geometry.

$n$	Lattice	HF				LDA-PZ	
		$E_p^n$	$E_p^2$	$E_d^{n-1}$	$E_f^n$	$E_p^2$	$E_f^n$
8	$P$	-428.221800	-107.055450	-328.590048	0.25672	-106.766415	0.33805
16	$F$	-856.443601	-107.055450	-756.811638	0.25693	-106.766415	0.33798
32	$I$	-1712.887207	-107.055450	-1613.255239	0.25693	-106.766415	0.33829
54	$F$	-2890.497155	-107.055450	-2790.865051	0.25707	-106.766415	0.33897
64	$P$	-3425.774381	-107.055449	-3326.142400	0.25695	-106.766415	0.33868
128	$F$	-6851.548839	-107.055451	-6751.916825	0.25698	-106.766414	0.33936
216	$P$	-11561.988593	-107.055450	-11462.356596	0.25696	-106.766415	0.33954
250	$F$	-13381.931279	-107.055450	-13282.299274	0.25697	-106.766415	0.33973
256	$I$	-13703.097661	-107.055450	-13603.465658	0.25697	-106.766415	0.33959

same basis set as for the bulk, except for the exponents of the two outer  $sp$  shells, which have been reoptimized variationally ( $\alpha=0.440$  and  $0.150$  instead of  $0.437$  and  $0.137$  bohr $^{-2}$ ).<sup>17</sup>

The LDA-PZ exchange-correlation potential is expanded in an auxiliary basis set of symmetrized atom-centered Gaussian type functions, with even-tempered exponents:<sup>18</sup> for Li $^+$  12  $s$  functions are used (the exponents span the  $0.15$ – $2000$  bohr $^{-2}$  range); for F $^-$  12  $s$  in the  $0.1$ – $2000$  bohr $^{-2}$  range and two  $p$  shells with  $0.3$  and  $0.9$  bohr $^{-2}$  exponents are used.<sup>19</sup>

As regards the computational conditions for the truncation of the Coulomb and exchange series, standard values as suggested in the CRYSTAL98 manual<sup>10</sup> have been used. The number of  $k$  points of the Brillouin zone where the Hamiltonian matrix is diagonalized will be discussed below. In order to obtain well converged results for the very small spin density at atoms far from the vacancy, the self-consistent field (SCF) convergence threshold on energy must be equal to  $10^{-7}$  hartree, or smaller.

The presence of the defect breaks the translational symmetry of the perfect crystal. In order to restore it (and thus to

be allowed to use a standard periodic code), the supercell scheme has been adopted: a multiple of the original primitive cell (which in the present case contains only two atoms) is built with the defect located at the center and is periodically repeated by the translation vectors of the supercell. The supercell must be large enough to satisfy the following conditions.

(1) The interaction between defects belonging to neighboring cells must be negligible; this includes both the direct interactions through Coulomb forces and the indirect interactions through the modification of the electronic structure of the atoms between the defects.

(2) All the atoms that relax from the perfect lattice position as a consequence of the presence of the defect must belong to the ‘‘reference’’ supercell and must be as far as possible unaffected by all other defects.

These two conditions mean that, in the case of a very well localized defect, all the neighbors within a given distance  $R$  from the defect must be included in the supercell; the actual value of  $R$  depends on the specific defect and on the screening properties of the medium. In the present case, however, two additional conditions are imposed.

TABLE II. Effect of the supercell size on the spin density  $\rho^{\alpha-\beta}$  (in units of  $10^{-2}$  bohr $^{-3}$ ) at the nuclei of the indicated atoms.  $XX$  indicates the anion vacancy; eight sets of neighbors are considered (I–VIII). Subscripts give the coordinates of the vacancy neighbors in units of the cation-anion distance ( $1.995$  Å).

$n$	$XX$	HF $\rho^{\alpha-\beta}$								
		I Li <sub>100</sub>	II F <sub>110</sub>	III Li <sub>111</sub>	IV F <sub>200</sub>	V Li <sub>210</sub>	VI F <sub>211</sub>	VII F <sub>220</sub>	VIII Li <sub>221</sub>	Li <sub>300</sub>
8	2.074	4.431	7.204	0.054						
16	2.080	2.272	3.641	0.021	0.143					
32	2.083	2.254	1.835	0.013	0.116	0.017				
54	2.082	2.255	1.837	0.006	0.022	0.008	0.034			0.000
64	2.083	2.255	1.829	0.007	0.044	0.009	0.038	0.096	0.000	
128	2.083	2.255	1.816	0.006	0.021	0.004	0.013	0.039	0.000	0.000
216	2.083	2.255	1.819	0.006	0.021	0.004	0.012	0.021	0.000	0.000
250	2.083	2.255	1.816	0.006	0.021	0.004	0.011	0.020	0.000	0.000
256	2.083	2.255	1.816	0.006	0.021	0.004	0.011	0.020	0.000	0.000

TABLE III. Effect of relaxation on the HF and LDA-PZ energies (in mhartree), on the spin density  $\rho^{\alpha-\beta}$  (in  $10^{-2}$  bohr $^{-3}$ ) at the  $F$  center position ( $XX$ ), and on the hyperfine coupling constants  $a$  and  $b$  (in MHz) at the nearest and next nearest neighbors.  $\Delta d$  (in Å) is the variation of the distance between the specified atom and the  $F$  center site; positive  $\Delta d$  means larger distance.  $\Delta E$  is the energy gain with respect to the unrelaxed geometry. First row data refer to the unrelaxed situation, second row to the relaxation of just the nearest neighbors, and third row to the nearest and the next nearest neighbor relaxation.

Atom	HF								LDA-PZ					
	$\Delta d$	$\Delta E$	$XX$ $\rho^{\alpha-\beta}$	$Li_{100}$		$F_{110}$		$\Delta d$	$\Delta E$	$XX$ $\rho^{\alpha-\beta}$	$Li_{100}$		$F_{110}$	
			$a$	$b$	$a$	$b$				$a$	$b$	$a$	$b$	
		0.00	2.04	38.80	3.13	76.26	11.14		0.00	1.66	41.78	3.04	116.25	13.63
$Li_{100}$	0.030	-0.70	1.99	36.40	3.02	81.93	11.35	0.022	-0.38	1.53	42.53	2.91	139.12	13.94
$F_{110}$	0.008	-0.86	2.00	36.78	3.02	80.44	11.30	0.004	-0.40	1.53	42.62	2.91	136.49	13.91

(3) As we are interested in the hyperfine coupling between the defect and its neighbors quite far from it, all these atoms need to be included in the region of no interaction with the defect of the next cell, i.e., they must be sufficiently far from the border of the cell.

(4) The supercell shape must be such as to exploit point symmetry of the defect as far as possible.

As regards the latter condition, cubic supercells can be obtained in three different ways starting from the primitive cell of LiF crystal, whose lattice is face-centered cubic ( $F$ ).

(i) Multiply the three translation vectors of the primitive cell by an integer  $n$ ;  $n=2,3,4$ , and 5 have been considered here, corresponding to supercells with 16, 54, 128, and 250 atoms. These cells will be indicated as  $S_{16}$ ,  $S_{54}$ ,  $S_{128}$ , and  $S_{250}$  and, like the primitive LiF cell, are rhombohedral with angles of 60°.

(ii) Use the conventional simple cubic cell ( $P$ ) of LiF, which contains eight atoms ( $S_8$ ); when its components are scaled by factors of 2 and 3, the  $S_{64}$  and  $S_{216}$  cells are obtained.

(iii) Build a primitive body-centered supercell ( $I$ ) starting from the supercell defined in point (ii) ( $S_8$ ) and scaling its components by a factor  $n$ . It is easily seen that odd  $n$  values do not generate translationally invariant replicas of  $S_2$ ;  $n=2$  and 4 generate  $S_{32}$  and  $S_{256}$ .

In summary, the following supercells have been considered in the present study:  $S_8$ ,  $S_{16}$ ,  $S_{32}$ ,  $S_{54}$ ,  $S_{64}$ ,  $S_{128}$ ,  $S_{216}$ ,  $S_{250}$ , and  $S_{256}$ .

The larger the supercell, the smaller its first Brillouin zone and thus the shrinking factor  $IS^{10}$  that defines the sampling frequency in  $k$  space. The adopted  $IS$  are 8, 8, 4, and 4 for  $S_8$ ,  $S_{16}$ ,  $S_{32}$ , and  $S_{54}$ , respectively, and 2 for larger cells; the corresponding number of  $k$  points is 35, 29, 8, 8, and 4 for  $S_{64}$  and  $S_{216}$  and 3 for  $S_{128}$ ,  $S_{250}$ , and  $S_{256}$ . With such a sampling, the total energy of the system is stable at least up to the sixth decimal figure (in hartree).

In order to be able to compare results obtained with supercells of increasing size, and thus to check the convergence of the properties of interest toward the noninteracting defect limit, the computational method must satisfy a size-consistency criterion: supercells of different size, for the perfect crystal, must provide the same value per LiF unit for all extensive properties. This condition is fulfilled by CRYSTAL98 when the computational conditions described above

are adopted; if applied to the total energy of the perfect system,  $E_p^n$ , the same energy per LiF unit is obtained ( $-107.05545$  and  $-106.76642$  hartree at the HF and LDA levels) up to the fifth decimal figure with all the supercells described above; this accuracy permits an unbiased comparison between the results obtained with different supercells (see Table I).

We are now in a position to verify condition (1) above, concerning the supercell size. The defect formation energy may be defined as

$$E_f^n = E_d^{n-1} + E_F - E_p^n$$

where  $E_d^{n-1}$  and  $E_F$  are the energy of the defective system and of the isolated fluorine atom.  $E_f^n$ , reported in Table I, turns out to converge quite rapidly as a function of  $n$ , the number of atoms in the supercell. The energy difference between the first and the last entries,  $S_8$  and  $S_{256}$ , is smaller than 0.5 (1.5) mhartree at the HF (LDA-PZ) level:  $E_f^n$  shows a quite modest stabilization, as a consequence of the reduced defect-defect interaction (see Table I).

In the next section it will be shown that relaxation is very small also for the nearest neighbors of the defect, so that condition (2) above is easily satisfied by a relatively small supercell. For the present study, however, condition (3) must also be considered, as we require well converged spin densities at the nuclei up to seventh nearest neighbors. Table II shows that only  $S_{216}$  ensures such a good convergence at the HF level. It is to be noted that beyond the seventh nearest neighbors the electron spin density is extremely small.

### III. RESULTS AND DISCUSSION

#### A. The geometry around the defect

Starting from the perfect lattice geometry (the equilibrium lattice parameters are 4.02 Å and 3.94 Å at the HF and LDA-PZ levels, respectively), the nearest and the next nearest neighbors of the defect are allowed to relax (Table III). They both move away from the defect; the amount of relaxation is small for  $Li_{100}$ , however, (0.030 Å and 0.022 Å for HF and LDA-PZ, respectively, with a corresponding energy gain of 1 and 0.4 mhartree) and negligible for  $F_{110}$  (0.008 and 0.004 Å for HF and LDA-PZ, with an energy gain of 0.2

TABLE IV. Effect of the basis set adopted for describing the  $F$  center on total HF and LDA-PZ energy and on the charge  $q^{\alpha+\beta}$  and the spin  $\rho^{\alpha-\beta}$  density at the vacancy site  $XX$  and at the nearest and next nearest neighbors.  $\Delta E$  (in mhartree) is the energy difference with respect to case 1, which refers to a calculation with the fluorine anion basis set centered at  $XX$ . In case 2 only the two most diffuse  $sp$  shells of the  $F^-$  basis set are kept. In case 3 only the most diffuse  $sp$  shell is kept and its exponent is reoptimized; in the third column a slash separates the best values of the exponents obtained for the HF and LDA-PZ methods. In case 4 the defect basis set is simplified to a single  $s$  function.

Case	Type	$\Delta E$	HF				LDA-PZ					
			$q_{XX}^{\alpha+\beta}$	$\rho_{XX}^{\alpha-\beta}$	$\rho_{Li_{100}}^{\alpha-\beta}$	$\rho_{F_{110}}^{\alpha-\beta}$	$q_{XX}^{\alpha+\beta}$	$\rho_{XX}^{\alpha-\beta}$	$\rho_{Li_{100}}^{\alpha-\beta}$	$\rho_{F_{110}}^{\alpha-\beta}$		
1	7-311( $s,sp,sp,sp$ )	0.00	0.91	2.19	2.25	1.88	0.00	0.78	1.74	2.46	2.92	
2	11( $sp,sp$ )	0.437 0.137	+0.10	0.90	1.94	2.26	1.88	+2.44	0.77	1.03	2.59	3.16
3	1( $sp$ )	0.093/0.073	-0.50	1.05	2.08	2.25	1.84	-1.09	0.97	1.48	2.58	3.19
4	1( $s$ )	0.093/0.073	-0.09	1.09	2.08	2.24	1.77	-0.15	1.02	1.48	2.57	3.18

and 0.02 mhartree, respectively). Relaxation of further neighbors is even smaller and is not reported.

Due to relaxation the spin density at the defect site decreases by about 2% and 8% for HF and LDA-PZ, respectively. These data confirm the density functional theory tendency to delocalize the unpaired electron far from the anion vacancy; this tendency is favored by the displacement of the nearest neighbors ( $Li_{100}$ ) away from the defect. The hyperfine constant  $b$  at the nearest and next nearest neighbors changes by less than 3% after relaxation, whereas  $a$  is slightly more sensitive to it (about 7% variation for  $Li_{100}$  and  $F_{110}$  at the HF level, 2% for  $Li_{100}$  and 20% for  $F_{110}$  at the LDA-PZ level).

On the basis of the relatively small effect of the geometry optimization on the energy and spin density data (with the exception of the Fermi contact term of  $F_{110}$  at the LDA-PZ level), all the data presented here refer to calculations performed at the experimental lattice parameter (3.99 Å) and unrelaxed geometry.

### B. The wave function of the unpaired electron of the $F$ center

The characteristics of the wave function describing the unpaired electron clearly emerge from the data reported in Table IV, where the effect of the modification of the basis set centered at the anion vacancy is explored. As a first guess, we used the same basis set as that used for the  $F^-$  ions of bulk LiF (case 1). The inner part of this basis set, describing the  $1s$  and  $2s$  electrons of  $F^-$ , is obviously useless as shown by case 2, when compared with case 1 (the energy changes by just 0.1 mhartree). This is also supported by the Mulliken population analysis, which gives charges very close to zero for the two inner shells of case 1; this is the case also for the valence shell with exponent  $0.437 \text{ bohr}^{-2}$ . In case 3 only the outer shell is kept and the corresponding exponent has been reoptimized: it varies from 0.137 to  $0.093 \text{ bohr}^{-2}$ , indicating that the unpaired electron in the  $F$  center is more diffuse than the valence electrons in the  $F^-$  valence shell, as a consequence both of their different symmetry ( $s$  for the  $F$  center and  $p$  for the valence electrons of  $F^-$ ) and of lack of nuclear attraction at the vacancy. Case 4 shows that  $p$  type orbitals give just a minor contribution (0.4 mhartree energy differ-

ence with respect to case 3). Eventually the defect wave function can be described by a single, diffuse  $s$  Gaussian very accurately.

The situation is very similar when the LDA-PZ approach is used, with the following exceptions (see second part of Table IV): (1) the  $s$  function is more diffuse, the best exponent being  $0.073 \text{ bohr}^{-2}$  instead of  $0.093 \text{ bohr}^{-2}$ ; (2) the  $p$  influence is larger (1 mhartree contribution to the energy instead of 0.4 in HF).

The amount of electronic charge that can be attributed to the vacancy according to a Mulliken analysis is very close to

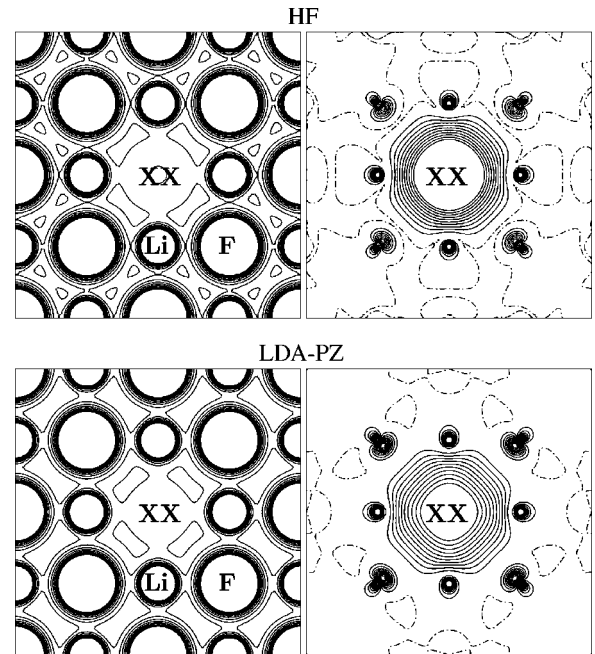


FIG. 1. Electron charge (left) and spin (right) density for an  $F$  center in LiF using the HF (top) and LDA-PZ (bottom) Hamiltonians. The section is parallel to the (100) plane through the defect. The unpaired electron is at the center of the map, whose side is  $7.98 \text{ \AA}$  long. The separation between contiguous isodensity curves is  $0.01$  and  $0.001 e/\text{bohr}^3$ , for the electron charge and spin density, respectively. The density range is  $0.01\text{--}0.1$  (left) and  $-0.01\text{--}0.01$  (right)  $e/\text{bohr}^3$ ; continuous, dashed, and dot-dashed lines denote positive, negative, and zero values.

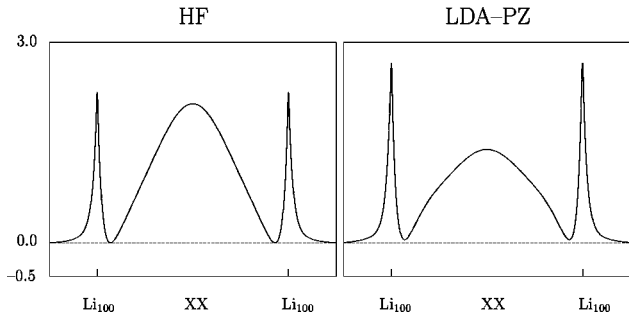


FIG. 2. Spin density profile (in  $10^{-2}e/\text{bohr}^3$ ) along the direction connecting the  $F$  center and the first neighbors  $\text{Li}_{100}$ . The path is  $5.985 \text{ \AA}$  long; ticks indicate nuclear positions.

1 (see  $q_{XX}^{\alpha+\beta}$  column). However, it is slightly higher in HF than in LDA, because of the above mentioned tendency of LDA-PZ to distribute spin density on different atoms. The last three columns give the spin density at the vacancy site and at the nearest and next nearest neighbor positions as a function of the basis set adopted. In general the basis set effect is small at the HF level and larger for LDA-PZ: the basis set optimization in this case favors the displacement of spin density away from the vacancy.

### C. Electronic structure

The effects of the removal of a F ion and the consequent formation of an  $F$  center are represented in the electron charge and spin density maps given in Fig 1. The maps on the left show that the deformation of the ions from their spherical shape is negligible; the Mulliken analysis confirms that charge transfer effects are also negligible: the six nearest Li neighbors and the 12 next nearest F neighbors have a HF net charge of  $+0.977|e|$  and  $-0.970|e|$ , respectively, which are very close to those of the perfect crystal  $\pm 0.976|e|$ . Higher order neighbors carry exactly the perfect crystal net charge. The LDA-PZ data for the two nearest neighbors are  $+0.965|e|$  and  $-0.968|e|$ , whereas the perfect crystal data are  $\pm 0.965|e|$ .

The localization of the unpaired electron at the anion vacancy is clearly evident at the center of the spin maps (Fig 1, right) and the spin polarization of the two nearest neighboring atoms is appreciable with both Hamiltonians. In Figs. 2

and 3 the spin density profiles along radial directions at the different neighboring nuclei are represented. They show that the spin density perturbation decreases with the distance from the  $F$  center in such a measure that from the third nearest neighbors it became necessary to magnify the scale; Li and F polarizations are quite different from each other, as a consequence of the  $s$  and  $p$  symmetry of the most diffuse functions; the Li peaks are always symmetric, whereas in the F case there are asymmetric twin peaks.

The presence of an unpaired electron is also revealed by the band structure of the defective system, given in Fig. 4 together with the one for the perfect crystal. The eigenvalues are plotted along two high symmetry paths in the Brillouin zone: from  $\Gamma(000)$  to  $X(\frac{1}{2}0\frac{1}{2})$  and from  $X$  to  $W(\frac{1}{2}\frac{1}{4}\frac{3}{4})$ . The  $2s$  and  $2p$  type valence bands and the bottom of the conduction band are shown. The bound unpaired electron level lies in the gap; the corresponding electron-hole level appears in the  $\beta$  spin structure, again in the gap but at positive energies. In the LDA-PZ case also, the two defective levels fall in the gap, but the energy difference is much smaller than the HF one.

### IV. THE HYPERFINE COUPLING CONSTANTS

Experimental evidence concerning the unpaired electron can be obtained by electron resonance techniques (EPR and ENDOR). Experiments provide useful information about the spin density distribution and geometry of the defects. A straight comparison between calculated and experimental data is possible for the hyperfine coupling constants  $a$  and  $b$  that determine the hyperfine structure of the spectra.<sup>5</sup> These constants appear in the formulation of the spin Hamiltonian in terms of which the ENDOR and EPR spectra are interpreted.

The isotropic ( $a$ ) and anisotropic ( $b$ ) hyperfine coupling constants for each nucleus  $N$  (in MHz) are expressed as<sup>20</sup>

$$a = \frac{2\mu_0}{3h} g\beta_e g_N \beta_n \rho^{\alpha-\beta}(0), \quad (1)$$

$$b = \frac{\mu_0}{4\pi h} g\beta_e g_N \beta_n [T_{11} - \frac{1}{2}(T_{22} + T_{33})], \quad (2)$$

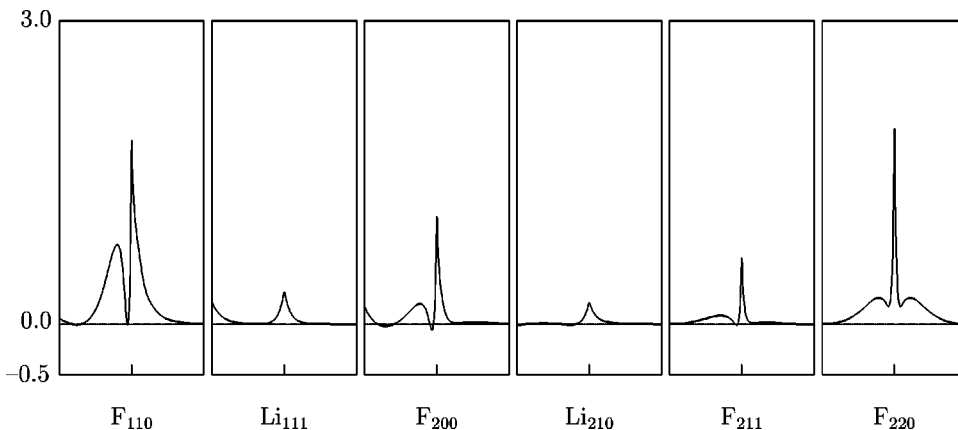


FIG. 3. Hartree-Fock spin density profile (in  $e/\text{bohr}^3$ ) along the direction connecting the  $F$  center and the specified atom. The path is  $1.995 \text{ \AA}$  long. Ticks indicate nuclear positions. Spin densities from  $\text{Li}_{111}$  to  $\text{F}_{220}$  are magnified by a factor of 50.

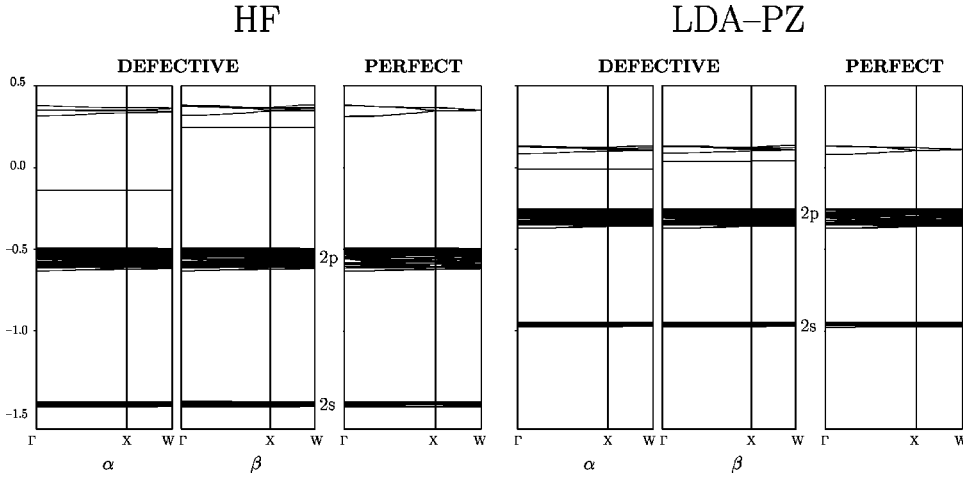


FIG. 4. Bottom conduction (positive energies) and valence (negative energies) bands of an  $F$  center in LiF as described at the  $S_{128}$  level.  $\alpha$  and  $\beta$  denote the majority and minority spin states, respectively. The  $S_{128}$  perfect LiF band structure is reported on the right for comparison. Energies in hartree.

where the spin density  $\rho^{\alpha-\beta}$  at  $N$ , the elements of the hyperfine coupling tensor  $\mathbf{T}$ , and the electron  $g$  factor are the only terms that depend on the electronic structure of the system (in our calculation we use the free electron  $g$  to approximate the true  $g$  factor, which is usually an acceptable approximation for our purposes). All other multiplicative factors in Eqs. (1) and (2) are tabulated constants<sup>20,21</sup> ( $h$  is the Planck constant,  $\beta_e$  and  $\beta_n$  the electronic and nuclear magnetons,  $\mu_0$  the permeability of the vacuum, and  $g_N$  the nuclear  $g$  factor).  $\mathbf{T}$  is a tensor of rank 2, which is obtained as the field gradient of the spin density at  $N$ . Its generic element has the form

$$T_{ij}^N = \sum_{\mu\nu} \sum_{\mathbf{G}} P_{\mu\nu\mathbf{G}}^{\text{spin}} \int \varphi_{\mu}(\mathbf{r}) \left( \frac{r^2 \delta_{ij} - 3r_i r_j}{r^5} \right) \varphi_{\nu}(\mathbf{r} - \mathbf{G}) d\mathbf{r} \quad (3)$$

where the origin of the Cartesian reference system is at nucleus  $N$ ,  $r_i$  denotes the  $i$ th component of  $\mathbf{r}$  and  $\varphi_{\nu}(\mathbf{r} - \mathbf{G})$  is the  $\nu$ th atomic orbital centered in cell  $\mathbf{G}$ .  $P_{\mu\nu\mathbf{G}}^{\text{spin}}$  is the direct space spin density matrix element connecting the  $\mu$ th atomic orbital in the zero cell (the reference cell) to the  $\nu$ th one in cell  $\mathbf{G}$ .  $T_{ii}$  in Eq. (2) are the elements of  $\mathbf{T}$  in diagonal form, following the convention that  $T_{11}$  is the maximum module component.

The calculated and experimental values of  $a$  for the coupling of the unpaired electron spin to nuclear spins are reported in Table V. HF usually underestimates the experimental values, with the sole exception of  $F_{200}$ , which is overestimated by nearly 100%. However, on the whole, the HF data show a qualitative agreement with experiment. Cal-

culated  $a$  values with LDA-PZ are of the same quality. However, in this case all constants are overestimated with the exception again of  $F_{200}$ .

The agreement for the  $b$  constant is much better than for  $a$  (see Table VI), in spite of the fact that the experimental values span about one order of magnitude (0.28 to 3.20 MHz). The largest HF percentage deviation is 23%, and it is about the same with LDA-PZ (here again the exception is  $F_{200}$ , but only as regards the LDA-PZ result, which is about 40% of the experimental value).

It must be stressed that the model Hamiltonian adopted for interpreting the experimental spectra assumes a tetragonal symmetry at all sites,<sup>5</sup> probably in order to reduce the number of parameters entering into the model. However only  $\text{Li}_{100}$ ,  $\text{Li}_{111}$ , and  $F_{200}$  have axial symmetry with respect to the line joining them to the vacancy. In all the other cases the  $\mathbf{T}$  tensor is fully characterized by the specification of a second constant  $c$  (the *asymmetry constant*), usually defined<sup>20</sup> as

$$c = \frac{\mu_0}{4\pi\hbar} g\beta_e g_N \beta_n \frac{1}{2} (T_{22} - T_{33}), \quad (4)$$

where  $\|T_{22}\| - \|T_{33}\|$  is non-negative. This asymmetry constant is given in Table VII, for future comparison. It turns out that  $c$  is a small (but not negligible) fraction of  $b$ .

Finally, the electric field gradient at the  ${}^7\text{Li}$  nuclei has been evaluated ( ${}^{19}\text{F}$ , whose natural abundance is 100%, having a nuclear spin of 1/2 is not active). The  $P$  value is small ( $-0.001$  MHz), as was the case for trapped holes<sup>13</sup> in MgO, CaO, and SrO with Li impurities, confirming that the local

TABLE V. Calculated and experimental (Refs. 5 and 6) hyperfine coupling constants  $a$  (in MHz) up to the seventh nearest neighbors of the vacancy.  $\delta$  is the percentage difference with respect to experiment.

$\hat{H}$	$a$						
	$\text{Li}_{100}$	$\text{F}_{110}$	$\text{Li}_{111}$	$\text{F}_{200}$	$\text{Li}_{210}$	$\text{F}_{211}$	$\text{F}_{220}$
HF	39.17	76.40	0.11	0.89	0.07	0.46	0.83
LDA-PZ	47.20	145.20	1.49	-0.05	0.42	2.56	3.55
Expt.	39.06	105.94	0.50	0.48	0.27	0.88	1.34
$\delta_{\text{HF}}\%$	+0.3	-27.9	-78.4	+85.2	-73.3	-48.0	-38.4
$\delta_{\text{LDA-PZ}}\%$	+20.8	+37.1	+197.2	-110.4	+55.6	+191.1	+165.0

TABLE VI. Calculated and experimental (Refs. 5 and 6) hyperfine coupling constants  $b$  (in MHz) up to the seventh nearest neighbors.  $\delta$  is the percentage difference with respect to experiment.

$\hat{H}$	$b$						
	Li <sub>100</sub>	F <sub>110</sub>	Li <sub>111</sub>	F <sub>200</sub>	Li <sub>210</sub>	F <sub>211</sub>	F <sub>220</sub>
HF	3.25	11.47	0.72	1.17	0.34	0.66	0.43
LDA-PZ	2.84	14.01	0.69	0.47	0.33	0.83	0.70
Expt.	3.20	14.96	0.68	1.12	0.28	0.69	0.56
$\delta_{HF}\%$	+1.5	-23.3	+5.7	+4.2	+21.8	-3.9	-22.7
$\delta_{LDA-PZ}\%$	-11.2	-6.4	+1.6	-57.7	+18.9	+19.9	+24.8

situation at the nearest neighbors is also only marginally perturbed with respect to the cubic situation.

## V. CONCLUSION

The electronic and magnetic properties of the  $F$  center in LiF have been investigated at the HF and LDA-PZ level. The influence of the supercell size with respect to the most important properties has been explored. It has been shown that CRYSTAL98 can provide very stable results, which permit one

TABLE VII. Calculated hyperfine coupling constants  $c$  (in MHz).

$\hat{H}$	$c$			
	F <sub>110</sub>	Li <sub>210</sub>	F <sub>211</sub>	F <sub>220</sub>
HF	0.38	0.00	0.03	0.07
LDA-PZ	0.76	0.00	0.11	0.03

to explore supercell convergence up to 256 atoms. At variance with defects, where the very localized nature of the defect in  $p$  or  $d$  type orbitals<sup>14,22</sup> cannot be described at the LDA-PZ level (in such cases only delocalized solutions are obtained), in the present case the LDA-PZ description is in qualitative agreement with experiment; on the whole, the HF and LDA-PZ deviations from experiment have opposite sign. A semiquantitative agreement is obtained with experiment for  $b$ , whereas for  $a$  only the trend is correctly reproduced.

New accurate experimental data would be welcome, including measurement of the  $c$  asymmetry constant and  $P$  electric field gradient tensor components, which are now available from calculation. This would permit a more complete comparison between theory and experiment.

\*Author to whom correspondence should be addressed. Email address: dovesi@ch.unito.it

<sup>1</sup>C.A. Hutchison, Phys. Rev. **75**, 1769 (1949).

<sup>2</sup>A.F. Kip, C. Kittel, R.A. Levy, and A.M. Portis, Phys. Rev. **91**, 1066 (1953).

<sup>3</sup>N.W. Lord, Phys. Rev. **105**, 756 (1957).

<sup>4</sup>N.W. Lord, Phys. Rev. Lett. **1**, 170 (1958).

<sup>5</sup>W.C. Holton and H. Blum, Phys. Rev. **125**, 89 (1962).

<sup>6</sup>H. Seidel and H. C. Wolf, *The Physics of Colour Centers* (Fowler, New York, 1968).

<sup>7</sup>B. Henderson, *Defects in Crystalline Solids* (Edward Arnold, Ltd., London, 1972).

<sup>8</sup>W.C. Holton, H. Blum, and C.P. Slichter, Phys. Rev. Lett. **5**, 197 (1960).

<sup>9</sup>C. Pisani, R. Dovesi, and C. Roetti, *Hartree-Fock ab initio Treatment of Crystalline Systems*, Vol. 48 of *Lecture Notes in Chemistry* (Springer Verlag, Heidelberg, 1988).

<sup>10</sup>V. Saunders, R. Dovesi, C. Roetti, M. Causà, N. M. Harrison, R. Orlando, and C. Zicovich-Wilson, computer code CRYSTAL98, Università di Torino, Torino, 1998.

<sup>11</sup>A. Lichanot, R. Orlando, G. Mallia, M. Merawa, and R. Dovesi, Chem. Phys. Lett. **318**, 240 (2000).

<sup>12</sup>A. Lichanot, Ph. Baranek, M. Merawa, R. Orlando, and R. Dovesi, Phys. Rev. B **62**, 12 812 (2000).

<sup>13</sup>A. Lichanot, C. Larrieu, C. Zicovich-Wilson, C. Roetti, R. Orlando, and R. Dovesi, J. Phys. Chem. Solids **59**, 1119 (1998).

<sup>14</sup>A. Lichanot, C. Larrieu, R. Orlando, and R. Dovesi, J. Phys. Chem. Solids **59**, 7 (1998).

<sup>15</sup>E. Aprà, in *Quantum-Mechanical ab initio Calculation of the Properties of Crystalline Materials*, Vol. 67 of *Lecture Notes in Chemistry*, edited by C. Pisani (Springer Verlag, Berlin, 1996), pp. 101–112.

<sup>16</sup>A. Zupan and M. Causà, Int. J. Quantum Chem. **56**, 337 (1995).

<sup>17</sup>[http://www.ch.unito.it/ifm/teorica/Basis\\_Sets](http://www.ch.unito.it/ifm/teorica/Basis_Sets)

<sup>18</sup>M. Towler, A. Zupan, and M. Causà, Comput. Phys. Commun. **98**, 181 (1996).

<sup>19</sup>[http://www.ch.unito.it/ifm/teorica/AuxB\\_Sets](http://www.ch.unito.it/ifm/teorica/AuxB_Sets)

<sup>20</sup>J. A. Weil, J. R. Bolton, and J. E. Wertz, *Electron Paramagnetic Resonance* (John Wiley & Sons, Inc., New York, 1994).

<sup>21</sup>*Handbook of Chemistry and Physics*, 72nd ed., edited by D. Lide (CRC Press, Boston, 1991–1992).

<sup>22</sup>R. Dovesi, R. Orlando, C. Roetti, and C. Pisani, Phys. Status Solidi B **217**, 63 (2000).